Noninvasive Average Flow and Differential Pressure Estimation for an Implantable Rotary Blood Pump Using Dimensional Analysis

Einly Lim, Dean M. Karantonis, *Student Member, IEEE*, John A. Reizes, Shaun L. Cloherty, *Member, IEEE*, David G. Mason, and Nigel H. Lovell*, *Senior Member, IEEE*

***Abstract*—Accurate noninvasive average flow and differential pressure estimation of implantable rotary blood pumps (IRBPs) is an important practical element for their physiological control. While most attempts at developing flow and differential pressure estimate models have involved purely empirical techniques, dimensional analysis utilizes theoretical principles of fluid mechanics that provides valuable insights into parameter relationships. Based on data obtained from a steady flow mock loop under a wide range of pump operating points and fluid viscosities, flow and differential pressure estimate models were thus obtained using dimensional analysis. The algorithm was then validated using data from two other VentrAssist IRBPs. Linear correlations between estimated and measured pump flow over a flow range of 0.5 to 8.0 L/min resulted in a slope of 0.98 ($R^2 = 0.9848$). The average flow error was 0.20 $\pm$ 0.14 L/min (mean $\pm$ standard deviation) and the average percentage error was 5.79%. Similarly, linear correlations between estimated and measured pump differential pressure resulted in a slope of 1.027 ($R^2 = 0.997$) over a pressure range of 60 to 180 mmHg. The average differential pressure error was 1.84 $\pm$ 1.54 mmHg and the average percentage error was 1.51%.**

***Index Terms*—Dimensional analysis, flow estimation, implantable rotary blood pump (IRBP), left ventricular assist device (LVAD).**

I. Introduction

THE VentrAssist (Ventracor, Ltd., Sydney, Australia) is a centrifugal implantable rotary blood pump (IRBP) with a hydrodynamic bearing that is used as a left ventricular assist device (LVAD) for long-term implant recipients [1]. Due to the insensitivity of IRBPs to preload, overpumping or underpumping conditions that endanger implant recipients might potentially occur if pump control is not properly implemented. This situation is further complicated by residual ventricular function, dependent on the amount of residual contractility and venous return [2], which causes pump head pressure to vary with each heart beat.

Manuscript received May 25, 2007; revised December 23, 2007. *Asterisk indicates corresponding author.*

E. Lim, S. L. Cloherty, and D. M. Karantonis are with the Graduate School of Biomedical Engineering, University of New South Wales, Sydney, New South Wales 2052, Australia.

*N. H. Lovell is with the Graduate School of Biomedical Engineering, University of New South Wales, Sydney, New South Wales 2052, Australia (e-mail: n.lovell@unsw.edu.au).

J. A. Reizes is with the School of Mechanical and Manufacturing Engineering, University of New South Wales, Sydney, New South Wales 2052, Australia.

D. G. Mason is with the Department of Surgery, Monash University, Victoria 3800, Australia, and also with the Department of Cardiothoracic Surgery, Alfred Hospital, Victoria 3181, Australia.

Digital Object Identifier 10.1109/TBME.2008.919723

Various pump control algorithms have been designed by different research groups. The traditional control strategy, which maintains a constant pump speed, demonstrates a limited degree of adaptability to cardiac demand and clinical conditions of the heart. Giridharan and Skliar [3] proposed that maintaining a constant average pressure difference (75 mmHg) between the left ventricle and the aorta provided sufficient physiological perfusion to the body over a wide range of physical activities and clinical cardiac conditions. On the contrary, Smith *et al.* [2] suggested that flow is a more physiologically relevant parameter than pump differential pressure since pump differential pressure by itself has no inherent physiological significance. Using a similar approach to Giridharan and Skliar [3], Wu *et al.* [4] based their algorithms on the control of aortic pressure rather than pump differential pressure. A state-space model of the human circulatory system as well as measurements of pump differential pressure was used to estimate the aortic pressure. The performance of all the aforementioned control algorithms (except speed control) requires accurate measurements of either pump flow or pump differential pressure. However, implantation of flow or pressure sensors in the body result in an attendant risk of thrombus formation, and the reliability of the measurements is affected by measurement drift, and thus, the need for *in situ* calibration.

Therefore, one design goal of an IRBP is to be able to reliably and accurately estimate pump flow as well as differential pressure without the need for additional implantable sensors. Extensive studies have reported that satisfactory algorithms for sensorless flow and differential pressure estimation through empirical process of pump variables (flow or differential pressure) mapping had been developed [5]–[8]. However, the performance and design characteristics of different pumps cause the proposed algorithms to be substantially different from each other [9]. In addition, to a large extent, the algorithms have failed to adequately model changes in fluid viscosity, and hence, blood hematocrit (HCT).

The present work involved an analysis of data obtained under steady flow conditions for a wide range of pump operating points and fluid viscosities, and employed a nondimensional analytical approach. By reducing the test data on a pump into nondimensional form, it is possible to extrapolate the performance of the pump with revised physical pump characteristics, different pump speeds, and different operating conditions [2]. Compared with purely empirical methods of flow or differential pressure mapping (where curve fitting is applied to the test

variables), the Buckingham π theorem [10], [11], which groups the test variables into fewer independent dimensionless groups, provides a better physical insight into the effects of different parameters on pump performance.

II. Methods

A. Mock Loop Experiments

The mock circulatory loop, consisting of a small reservoir bag (200 mL), the VentrAssist pump, a variable resistance clamp, and two segments of silicone tubing (1.5 m total length, 3/8-in inner diameter, 3/32-in thickness): one connecting the pump outlet to the reservoir and the other connecting the reservoir back to the pump inlet, provided a test environment for steady flow conditions. The pump flow rate, pump differential pressure, impeller speed and electrical input power were recorded at each operating point during the experiment at a sampling rate of 4 kHz. The fluid employed in the experiment was an aqueous glycerol solution at concentrations of 30%wt (2.323 mPas), 39%wt (3.394 mPas), and 45%wt (4.823 mPas). In each case, a resistance clamp mounted on the loop was adjusted so as to vary the circuit resistance. The circuit resistance was defined by adjusting the resistance clamp to achieve a certain flow level, e.g., 1, 3, 5, 7, 9 L/min at a fixed speed, i.e., 2300 r/min. At each resistance level, pump speed was adjusted in increments of 100 r/min within a range of 1800–3000 r/min. Once the desired speed had been set and the pump speed controller showed a steady pumping condition, values of pump power, speed, differential pressure, and flow rate averaged over a 20-s period were recorded. Since the viscosity of aqueous glycerol is highly sensitive to temperature, a thermistor transducer was attached to the loop to measure and control the temperature of the solution. The temperature was maintained at 25 °C. Three versions of nominally the same VentrAssist pumps were used to obtain the data, one set for each pump. The dataset from the first pump was used in the derivation of the correlation, while the other two datasets were used as validation. The raw data from pump 1 for an aqueous glycerol solution with a concentration of 39%wt is shown in Figs. 1 and 2. It can be seen that once the speed and power is known, the flow and differential pressure across the pump can be immediately determined. Unfortunately, if the fluid is changed, the curves are also changed; therefore, a more general approach needs to be provided.

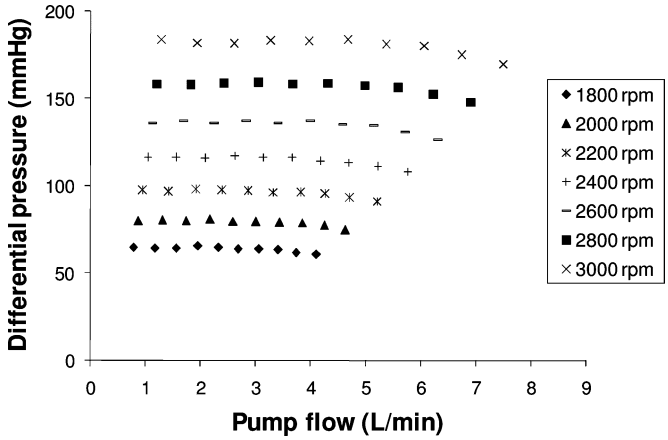

Fig. 1. Graph of differential pressure versus flow for various speeds at a constant viscosity (39%wt aqueous glycerol).

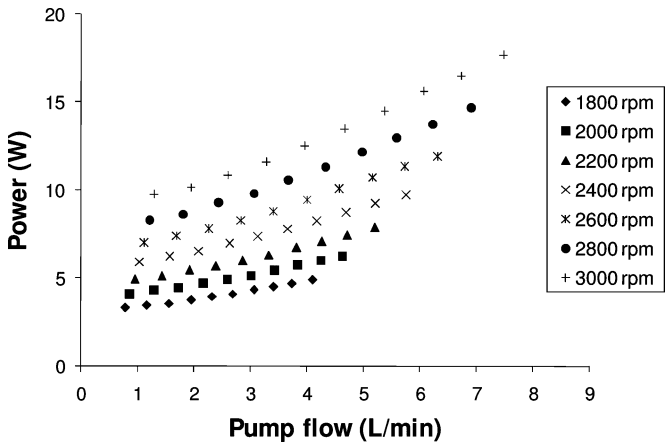

Fig. 2. Graph of input power versus flow for various speeds at a constant viscosity (39%wt aqueous glycerol).

B. Theoretical Framework

The objective was to use the viscosity of the aqueous glycerol solution (as a blood analogue at known HCT), pump input power, and impeller speed as indicators of pump flow rate and differential pressure. Ideally, the electromagnetic energy supplied by the external power source is converted into the fluid energy for the pump as well as the inertial energy used to accelerate or decelerate the impeller. However, in a practical situation, various losses occur along the flow passage path in the pump. The energy losses in a general pump include mechanical losses caused by mechanical contact at the shaft sealing section, disk friction losses consumed with friction torque in the gap between the impeller shroud disk and the pump housing wall, fluid leakage losses caused by recirculation of the fluid, and hydraulic losses in the impeller and in the diffuser (such as flow separation) [12].

Due to the complexity in the analysis of the pump characteristics caused by various operating losses and imperfections involved in the design, the theoretical relationship between power, flow, and differential pressure derived for an ideal centrifugal pump is not applicable when studying their practical performance. Thus, the current approach aims to use a systematic nondimensional approach that is applicable to any pump design to derive the relationship between pump power, speed, fluid viscosity, flow, and differential pressure.

The performance of a turbomachine depends on a number of variables, including pump differential pressure (Δp), input power (P), and efficiency

$$\Delta p = f_1(\omega, Q, \mu, \rho, D, l_1, \ldots, l_m, \alpha_1, \ldots, \alpha_n) \quad (1)$$

$$P = f_2(\omega, Q, \mu, \rho, D, l_1, \ldots, l_m, \alpha_1, \ldots, \alpha_n). \quad (2)$$

As shown in (1) and (2), Δp and P depend on the speed of the impeller (ω), flow rate through the pump (Q), viscosity (μ),

TABLE I
DEFINITION OF THE NONDIMENSIONAL GROUPS THAT ARE SPECIFICALLY APPLICABLE TO PUMPS

Symbol	Definition	
Ψ	pressure coefficient	$c_{\psi}.\frac{\Delta p}{\rho.\omega^2.D^2}$
Φ	flow coefficient	$c_{\Phi}.\frac{Q}{\omega.D^3}$
Π	power coefficient	$c_{\Pi}.\frac{P}{\rho.\omega^3 D^5}$
Re	Reynolds number	$c_{\mathrm{Re}}.\frac{\rho.\omega.D^2}{\mu}$

and density (ρ) of the fluid, as well as the geometric parameters of the pump, which include the characteristic dimension of the pump represented by the impeller diameter (D), lengths (l), and angles (α) required to fully describe the pump body and rotor. The Buckingham π theorem can be used to reduce the number of variables involved in determining the performance of the pump to a smaller number of nondimensional groupings.

Using dimensional analysis as explained in Appendix A, together with justified assumptions, (1) and (2) can be rewritten as the pump affinity laws

$$\frac{\Delta p}{\rho\omega^2 D^2} = F_3\left(\frac{Q}{\omega D^3}, \frac{\rho\omega D^2}{\mu}\right) \tag{3}$$

and

$$\frac{P}{\rho\omega^3 D^5} = F_4\left(\frac{Q}{\omega D^3}, \frac{\rho\omega D^2}{\mu}\right). \tag{4}$$

The nondimensional groups are listed in Table I, which are specifically applicable to the types of pumps discussed in this paper. Table II lists the units and corresponding constants leading to truly nondimensional coefficients.

TABLE II
UNITS AND CORRESPONDING CONSTANTS THAT RESULT IN TRULY NONDIMENSIONAL COEFFICIENTS

Symbol	Definition	Unit/Constant
Δp	pump differential pressure	[mmHg]
Q	pump flow	[L/min]
P	pump input power	[W]
ω	pump speed	[rpm]
μ	dynamic viscosity	[$kgm^{-1}s^{-1}$]
ρ	fluid density	[kgm^{-3}]
D	pump impeller diameter	[cm]
$l_1.....l_m$	lengths required to fully describe the pump body and rotor	[cm]
$\alpha_1.... \alpha_n$	angles required to fully describe the pump body and rotor	[rad]
c_{Ψ}	pressure coefficient constant	1.2158 x 10^5 $\left[\frac{(Pa/mmHg)}{(kgm^{-3}/gcm^{-3}).(rads^{-1}/rpm)^2.(m/cm)^2}\right]$
c_{Φ}	flow coefficient constant	159.161 $\left[\frac{(m^3s^{-1}/L\min^{-1})}{(rads^{-1}/rpm).(m/cm)^3}\right]$
c_{Π}	power coefficient constant	8.7082 x 10^9 $\left[\frac{1}{(kgm^{-3}/gcm^{-3}).(rads^{-1}/rpm)^3.(m/cm)^5}\right]$
c_{Re}	Reynolds number constant	0.01 $\left[\frac{(kgm^{-3}/gcm^{-3}).(rads^{-1}/rpm).(m/cm)^2)}{1}\right]$
ω_d	design speed	2400 rpm

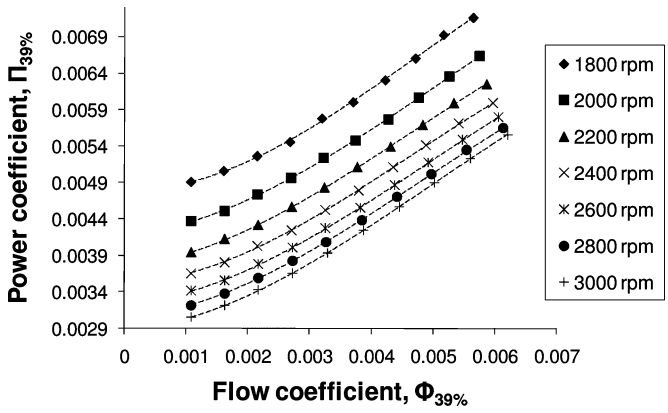

Fig. 3. Graph of power coefficient ($\Pi_{39\%}$) versus flow coefficient ($\Phi_{39\%}$) for various speeds at a constant viscosity (39%wt aqueous glycerol). It is observed that the power coefficient values are spread by more than $\pm 25\%$ from the mean.

C. Data Analysis

1) Flow estimate model: In the first step of the dimensional analysis, a graph of power coefficient versus flow coefficient was plotted for various speeds at a constant viscosity (39%wt aqueous glycerol) (see Fig. 3). Dynamic viscosity of 39%wt aqueous glycerol solution at 25 °C, 3.4 mPas, is very close to that of the average viscosity of whole human blood, 3.2 mPas, with hematocrit level of 38% at 37 °C [13]. Instead of collapsing onto a single curve, it was observed that the power coefficient values spread was more than $\pm 25\%$ from the mean for the speeds plotted. This was due to the fact that the coil winding and other friction losses did not follow the same pattern as the power required to move the fluid, and that the Reynolds number changed as the speed was altered. Thus, power coefficients needed to be corrected for varying speed (since viscosity did not vary in the training dataset used).

As may be observed in Fig. 3, an empirically derived cubic relationship between power coefficients and flow coefficients was obtained at each speed, namely

$$\Pi_{39\%} = a\Phi_{39\%}^3 + b\Phi_{39\%}^2 + c\Phi_{39\%} + d. \tag{5}$$

Since the speed generally causes an offset in the graph, a, b, and c are assumed to be constant, while d is a function of speed (ω). A plot of d against ω indicated that d is inversely

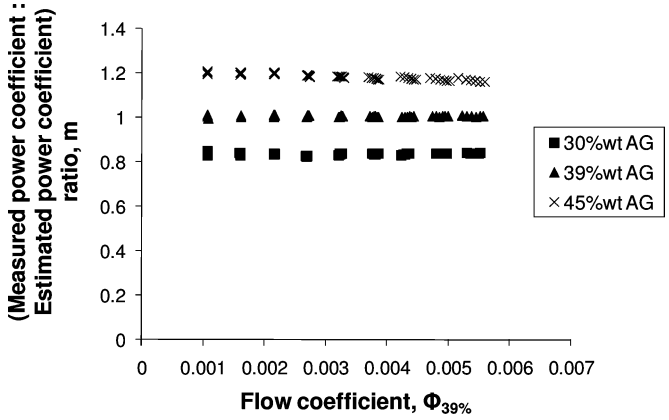

Fig. 4. Ratio of measured power coefficients to estimated power coefficients (m) versus flow coefficient (Φ). As viscosity increases, higher power coefficients are needed to produce the same flow coefficients.

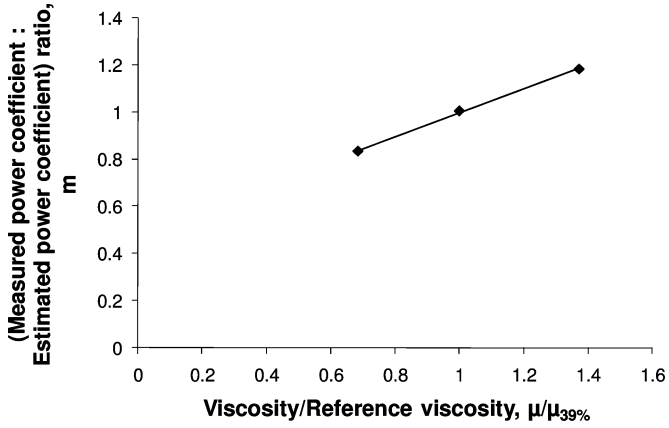

Fig. 5. Graph of power coefficient ratio (m) versus relative viscosity ($\mu/\mu_{39\%}$) shows a linear relationship between them.

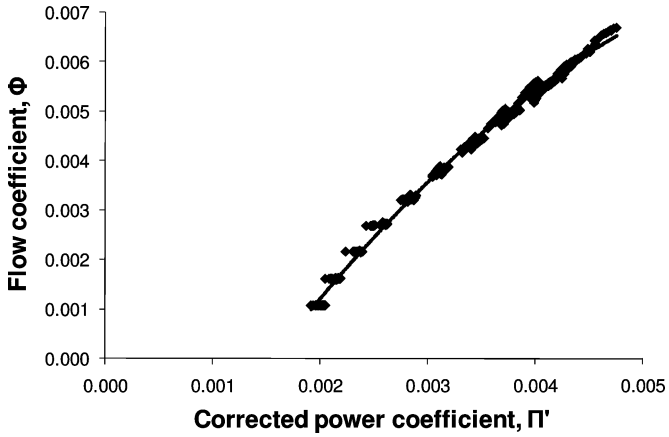

Fig. 6. Graph of flow coefficient (Φ) versus corrected power coefficient (Π'). Estimates of flow can be obtained from the equations relating the two variables.

proportional to ω^2, so that the following relationship was obtained:

$$\Pi_{39\%} = -7148.9\Phi_{39\%}^3 + 104.4\Phi_{39\%}^2 + 0.057\Phi_{39\%} + 0.0018 + \frac{0.001642}{(\omega_{39\%}/\omega_d)^2}. \quad (6)$$

To study the effect of viscosity, two other sets of training data (obtained using 30%wt and 45%wt aqueous glycerol solution) were used. Equation (6) was used to estimate power coefficients for each training data set. The ratio, m, of measured power coefficients to estimated power coefficients predicted by (6) was calculated from

$$m = \frac{\text{Measured power}}{\text{Estimated power}} = \frac{\Pi}{a\Phi^3 + b\Phi^2 + c\Phi + d}. \quad (7)$$

It is evident from Fig. 4 that the ratio did not collapse to the value of 1.0 when viscosity of the solution changed. The data for each viscosity showed a different and approximately constant power coefficient ratio. As viscosity increased, higher power coefficients were required to produce the same flow coefficient due to the effect of viscosity on the Reynolds number.

The relationship between the power coefficient ratio, m, and viscosity, μ, is shown in Fig. 5 and given by

$$m = 0.5067\frac{\mu}{\mu_{39\%}} + 0.4918. \quad (8)$$

In order to collapse the set of $\Pi - \Phi$ curves in Fig. 3 onto a single curve for all viscosities and speeds, the power coefficient was corrected to

$$\Pi' = \frac{\Pi}{m} - d. \quad (9)$$

Since the aim of this paper is the development of a method of estimating the flow rate from power and speed measurements, flow coefficients, Φ, were plotted against corrected power coefficients, Π', in Fig. 6, together with the line of best fit

$$\Phi = -241.19\Pi'^2 + 3.556\Pi' - 0.0049. \quad (10)$$

2) Differential pressure estimate model: As in Section II-C1, a graph of differential pressure coefficient versus flow coefficient was plotted for various speeds at a constant viscosity (39%wt aqueous glycerol) (see Fig. 7). It was observed that there was only a small spread of differential pressure coefficient values at the same value of flow coefficient. This indicates that there is negligible effect of the Reynolds number on the pump characteristic ($\Psi - \Phi$) curve.

To study the effect of viscosity, two other sets of training data (obtained using 30%wt and 45%wt aqueous glycerol solution) were used. It is shown in Fig. 8 that the curves for various viscosities collapse onto a curve with only a small spread. A cubic relationship obtained between differential pressure coefficients and flow coefficients

$$\Psi = -170959\Phi^3 + 1024\Phi^2 - 1.7444\Phi + 0.1528 \quad (11)$$

is also shown in Fig. 8.

III. Results

Flow and differential pressure estimate equations were developed by applying the methodology described before to a training data set. The performance of the estimation models

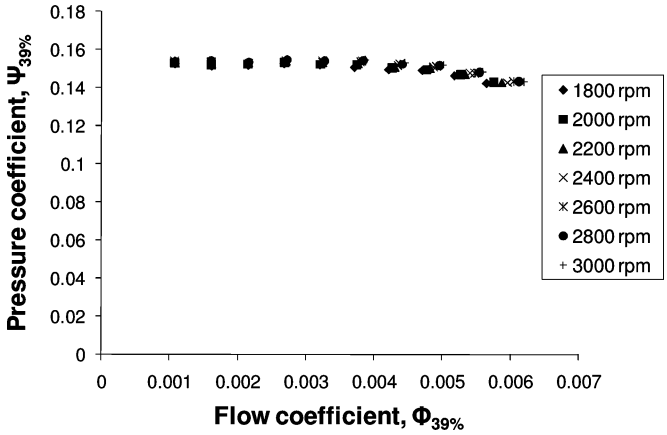

Fig. 7. Graph of pressure coefficient ($\Psi_{39\%}$) versus flow coefficient ($\Phi_{39\%}$) for various speeds at a constant viscosity (39%wt aqueous glycerol). It was observed that there is only a small spread of differential pressure coefficient values at the same value of flow coefficient.

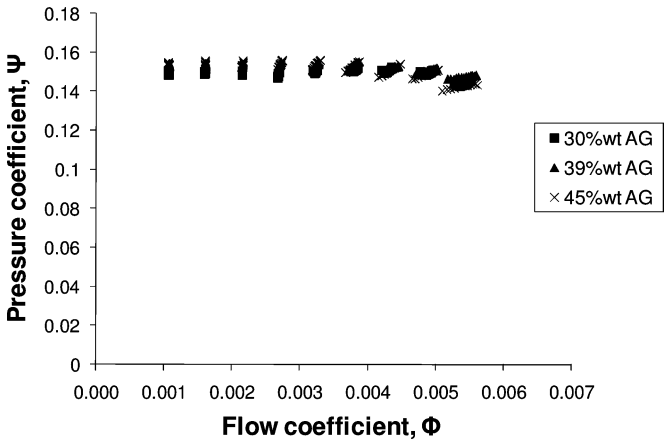

Fig. 8. Graph of pressure coefficient (Ψ) versus flow coefficient (Φ) for various viscosities (30%wt, 39%wt and 45%wt aqueous glycerol). It was shown that viscosity has a negligible effect on the Ψ–Φ curves.

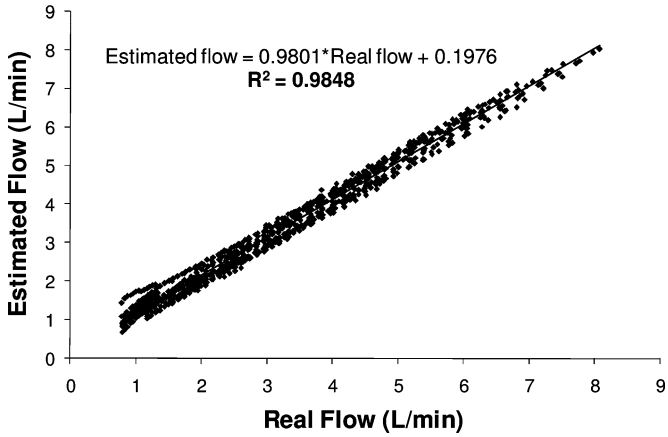

Fig. 9. Graph of estimated flow versus real flow corresponding to a range of measured flow rates (0.5–8 L/min). The performance of the flow estimate equation derived using the training dataset was validated against the testing dataset obtained using two other VentrAssist pumps having similar hydraulic characteristics.

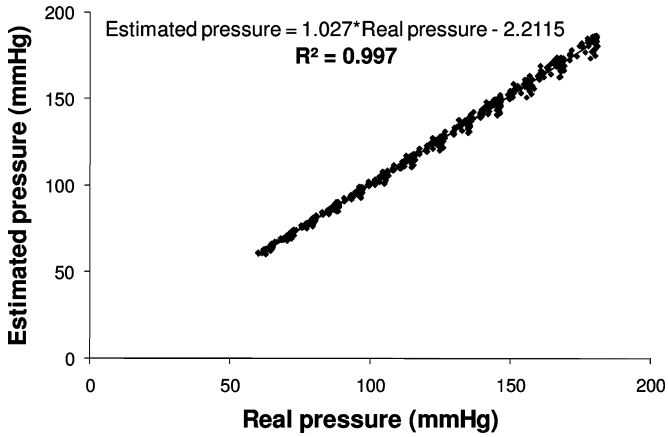

Fig. 10. Graph of estimated differential pressure versus real differential pressure corresponding to a range of measured differential pressure (60–180 mmHg). The performance of the differential pressure estimate equation derived using the training dataset was validated against the testing dataset obtained using two other VentrAssist pumps having similar hydraulic characteristics.

was then validated against the remaining pool of data obtained using two other VentrAssist pumps, which cover the same viscosity levels as the training data. Fig. 9 illustrates the estimated flow corresponding to a range of measured flow rates (0.5–8.0 L/min), while Fig. 10 illustrates the estimated differential pressures corresponding to a range of measured differential pressures (60–180 mmHg). Correlation between measured and estimated flow, as well as between measured and differential pressure was highly significant (flow: $R^2 = 0.9848$; differential pressure: $R^2 = 0.997$), and the slope of the linear regression line was very close to unity (flow: slope $= 0.98$; differential pressure: slope $= 1.027$). The residual error for flow estimation was in the range ± 0.8 L/min, while for differential pressure lay within the range of ± 8 mmHg. The average flow error was 0.20 $\pm$ 0.14 L/min (mean $\pm$ standard deviation), and the average differential pressure error was 1.84 $\pm$ 1.54 mmHg.

IV. Discussion

Noninvasive estimation of average pump flow and differential pressure has been investigated by many research groups as a means for physiological control of IRBPs. Most research groups have used surface fitting to map flow from the measurable quantities, e.g., power and speed. Bertram [5] reported that the first successful attempt at flow estimation was demonstrated by Wakisaka *et al.* [14] using pump power, speed, and HCT level. They derived their algorithm from the data obtained in a mock loop setup using whole goat blood, and successfully validated it in a healthy goat with an average error of 0.5 L/min over a range of 2.3–8.1 L/min. As Malagutti *et al.* [9] indicated, the limitation of their study was that the effects of viscosity were investigated at only a single target speed (2800 r/min).

On the other hand, Tsukiya *et al.* [12] included an extra step to estimate viscosity by occluding the pump outlet ($Q = 0$) for $<$10 s, based on an inverse linear correlation between the Reynolds number and the speed-normalized current at zero flow. The algorithm achieved a maximum error of 0.5 L/min between estimated and measured flow and 15 mmHg between estimated and measured differential pressure when tested in sheep. The

limitation of their study is the infeasibility of regular pump outlet occlusion in patients.

Tsukiya *et al.* [15] developed a technique for estimating the instantaneous flow rate in a pump implanted chronically in an animal. The technique took into account reverse flow, inlet cannula obstruction, and suction. They reported a mean flow rate error of 1 L/min. The main difference between their study and the present investigation is that they used a centrifugal pump rotor supported by a thrust bearing that contains the mechanical contacting surface, while the present study utilizes pumps that are hydraulically supported. Therefore, viscous friction losses have a much more significant influence in the present study as compared with their study, where the mechanical friction losses and the electromagnetic losses were dominant.

Previously, in our laboratory, we developed a steady-flow-estimation model based on a VentrAssist pump, taking into account the effect of blood HCT [9]. We reported a residual error of 0.25 ± 0.2 L/min. The current approach yields a slightly higher accuracy (with average flow estimation residuals of 0.21 ± 0.15 L/min). Given the spread of the residuals, this difference is not statistically significant. More significantly, in the present paper, the model is validated against data obtained using two VentrAssist pumps, which are slightly different from each other due to inevitable variations in tolerances incurred in the manufacturing process. The advantage of the current approach is that we can obtain a more fundamental understanding of how different fluid mechanical parameters affect the pump performance, and, if required, ascertain the performance of the pump under modified operating conditions.

It is important to note that the performance of the pressure estimate model derived in the present paper degrades when the flow coefficient increases. This is due to the fact that at a higher speed (or higher Reynolds number), the curves shift to the right, indicating that the pump is able to deliver a higher flow rate at the same differential pressure. In order to collapse the $\Psi - \Phi$ curves into a single curve, Wong *et al.* [16] proposed that the differential pressure be plotted against a modified flow coefficient. However, the method does not seem to improve the present pressure estimate model, probably due to the fact that the error in the pressure estimation is not only a function of Reynolds number, but also a function of flow coefficient [17]. As stated by Lorenz and Smith [17], the commonly used definition of the Reynolds number, which uses the impeller speed as the representative velocity, might not hold true at operating points far from the pump's optimal efficiency point. Since the spread of the differential pressure at the same flow coefficient is considered small in our flow range of interest (0.5–8 L/min), no further effort has been taken to refine the equation by collapsing the curves.

Several approaches [12], [18] have been proposed to estimate HCT level in the clinical setting, since variation in HCT level may cause differences in flow rates as high as 2 L/min at the same power and speed. Unfortunately, research to date has not been particularly successful. For example, Kitamura *et al.* used physical models of the motor, the centrifugal pump, and the Windkessel model of the systemic circulation to solve for viscosity, pump flow, and pressure [18]. The estimated viscosity converged to the true value *in vitro*, but failed *in vivo*. The estimates vary between 8 and 13 cP depending on the driving conditions, while the actual blood viscosity was about 2.8 cP. The uncertainty in the estimation of viscosity *in vivo* was probably due to the oversimplification of the systemic circulation model. In our present study, it is assumed that in the clinical setting, the HCT level will be ascertained by prior measurement. Future studies shall examine the noninvasive estimation of HCT level in the patients' circulation using the implanted pump as a sensing device.

The present study uses aqueous glycerol solution instead of blood. Since blood is a non-Newtonian fluid, it is expected to complicate the estimate of flow using power. However, at the high shear rates experienced in the VentrAssist IRBP, i.e., $>1000\ \mathrm{s}^{-1}$, the dynamic viscosity of blood can be considered to be independent of shear rate [7].

It should be noted that the present study focuses on the estimation of flow rate under steady flow conditions. In a pulsatile environment such as the cardiovascular system, the inertia of the fluid, the pump's rotating element, and the time constants of the speed controller need to be taken into account. The electrical input power will not only be used to provide the torque to the pump, but will also be used to accelerate or decelerate the impeller. Thus, a term that takes into account the moment inertia of the impeller has to be added. Furthermore, the time taken by the controller to sense and respond to load changes is important in developing the dynamic pump model. Experimentation on these aspects of instantaneous flow estimation is ongoing in our laboratory. Results from the experiments showed that average flow estimates are applicable to pulsatile flow environments, in the time-averaged sense [19]. This is in good agreement with the excellent results which are obtained in water hammer calculations when power supply is cut to very large pumps.

V. Conclusion

The work herein introduces a systematic approach based on dimensional analysis to estimate average flow rate from average pump input power, average speed, and viscosity. In comparison with empirical model fitting, this approach proves to be more accurate, while also providing valuable insights into relationships between various fluid mechanics parameters that affect the pump flow estimated.

Appendix A

The performance of a turbomachine depends on a number of variables, including pump differential pressure (Δp), input power (P), and efficiency. Since the present work aims to estimate flow and differential pressure across the pump from the pump input power, fluid viscosity, and impeller speed, we need at least two equations, one for the total pressure rise across the pump, Δp, and another for power required to drive the pump, P. Δp and P depend on the speed of the impeller (ω), flow across the pump (Q), viscosity of the fluid (μ), as well as the geometric parameters of the pump, which include pump impeller diameter (D), lengths (l), and angles (α) required to fully describe the

pump body and rotor.

$$\Delta p = f_1(\omega, Q, \mu, \rho, D, l_1, \ldots, l_m, \alpha_1, \ldots, \alpha_n) \quad (12)$$

$$P = f_2(\omega, Q, \mu, \rho, D, l_1, \ldots, l_m, \alpha_1, \ldots, \alpha_n). \quad (13)$$

Buckingham's π theorem was used to reduce the number of variables in (12) and (13) into a smaller number of nondimensional groupings [10], [11]. The theorem states that: Given a relation among *j* parameters of the form

$$q_1 = f_1(q_2, q_3, \ldots, q_j)$$

the *j* parameters may be grouped into *j-r* independent dimensionless parameters in the form of

$$\Pi_1 = F_1(\Pi_2, \Pi_3, \ldots, \Pi_{j-r})$$

where *r* is usually equal to the minimum number of independent dimensions, called repeating variables, required to specify the dimensions of all the parameters.

In the first step of the derivation, ρ (dimension $= ML^{-3}$), ω (dimension $= T^{-1}$), and *D* (dimension = *L*) were selected as a set of repeating variables since it includes all the primary dimensions, i.e., MLT. Equations (12) and (13) were then transformed into nondimensional forms, i.e., (14) and (15), by dividing each dimensional term in the equations by a combination of the repeating variables taken to appropriate powers

$$\frac{\Delta p}{\rho\omega^2 D^2} = F_1\left(\frac{Q}{\omega D^3}, \frac{\rho\omega D^2}{\mu}, \frac{l_1}{D}, \ldots, \frac{l_m}{D}, \alpha_1, \ldots, \alpha_n\right) \quad (14)$$

$$\frac{P}{\rho\omega^3 D^5} = F_2\left(\frac{Q}{\omega D^3}, \frac{\rho\omega D^2}{\mu}, \frac{l_1}{D}, \ldots, \frac{l_m}{D}, \alpha_1, \ldots, \alpha_n\right). \quad (15)$$

Since attention is limited to a single model of a rotary centrifugal blood pump, the geometrical parameters are in principle the same for all copies of the pump, so (14) and (15) reduce to

$$\frac{\Delta p}{\rho\omega^2 D^2} = F_3\left(\frac{Q}{\omega D^3}, \frac{\rho\omega D^2}{\mu}\right) \quad (16)$$

$$\frac{P}{\rho\omega^3 D^5} = F_4\left(\frac{Q}{\omega D^3}, \frac{\rho\omega D^2}{\mu}\right). \quad (17)$$

Thus, complete similarity in pump performance tests would require identical flow coefficients and Reynolds numbers. Since the flow through the clearances is controlled by different physical phenomena to those involved in pumping, it has been suggested that a number of Reynolds numbers may be needed to fully describe the flow in a pump.

In practice, the viscous effects (Reynolds numbers) are unimportant for fully turbulent flow. The conventional laminar-to-turbulent flow transition value for the pump Reynolds number is approximately 2 000 000 (scaled from 500 000 to account for difference in Reynolds number definition) [20]. However, since blood pumps usually operate in or near the laminar flow region [2], with a relatively low Reynolds number (65 000–220 000 for our test data), viscosity effects have to be taken into account. Furthermore, since the measured input power is the power supplied by the controller to the motor coils, electromechanical power consumption, which largely depends on the motor speed, needs to be considered.

REFERENCES

[1] D. Esmore, D. Kaye, R. Salamonsen, M. Buckland, M. Rowland, J. Negri, Y. Rowley, J. Woodard, J. Begg, and P. Ayre, "First clinical implant of the VentrAssist left ventricular assist system as destination therapy for end-stage heart failure," *J. Heart Lung Transplant*, vol. 24, pp. 1150–1154, 2005.

[2] W. A. Smith, M. Goodin, M. Fu, and L. Xu, "System analysis of the flow/pressure response of rotodynamic blood pumps," *Artif. Organs*, vol. 23, pp. 947–955, 1999.

[3] G. A. Giridharan and M. Skliar, "Control strategy for maintaining physiological perfusion with rotary blood pumps," *Artif. Organs*, vol. 27, pp. 639–648, 2003.

[4] Y. Wu, P. Allaire, G. Tao, and D. Olsen, "Study of pressure estimation for a human circulatory system with a LVAD," in *Proc. 2006 Amer. Control Conf.*, pp. 713–718.

[5] C. Bertram, "Measurement for implantable rotary blood pumps," *Physiol. Meas.*, vol. 26, pp. R99–R117, 2005.

[6] M. Yoshizawa, T. Sato, A. Tanaka, K. Abe, H. Takeda, T. Yambe, S. Nitta, and Y. Nose, "Sensorless estimation of pressure head and flow of a continuous artificial heart based on input power and rotational speed," *ASAIO J.*, vol. 48, pp. 443–448, 2002.

[7] P. J. Ayre, N. H. Lovell, and J. C. Woodard, "Non-invasive flow estimation in an implantable rotary blood pump: A study considering non-pulsatile and pulsatile flows," *Physiol. Meas.*, vol. 24, pp. 179–189, 2003.

[8] A. Funakubo, S. Ahmed, I. Sakuma, and Y. Fukui, "Flow rate and pressure head estimation in a centrifugal blood pump," *Artif. Organs*, vol. 26, pp. 985–990, 2002.

[9] N. Malagutti, D. M. Karantonis, S. L. Cloherty, P. J. Ayre, D. G. Mason, R. F. Salamonsen, and N. H. Lovell, "Non-invasive average flow estimation for an implantable rotary blood pump: a new algorithm incorporating the role of blood viscosity," *Artif. Organs*, vol. 31, pp. 45–52, 2007.

[10] R. W. Fox and A. T. McDonald, *Introduction to Fluid Mechanics*, 6th ed. New York: Wiley, 2004, pp. 273–300.

[11] E. Buckingham, "On physically similar systems: Illustrations of the use of dimensional equations," *Phys. Rev.*, vol. 4, no. 4, pp. 345–376, Oct. 1914.

[12] T. Tsukiya, T. Akamatsu, K. Nishimura, T. Yamada, and T. Nakazeki, "Use of motor current in flow rate measurement for the magnetically suspended centrifugal blood pump," *Artif. Organs*, vol. 21, pp. 396–401, 1997.

[13] A. C. Guyton and J. E. Hall, *Textbook of Medical Physiology*, 9th ed. Philadelphia, PA: Saunders, 1996, pp. 168.

[14] Y. Wakisaka, Y. Okuzono, Y. Taenaka, K. Chikanari, T. Masuzawa, T. Nakatani, E. Tatsumi, T. Nishimura, Y. Takewa, T. Ohno, and H. Takano, "Noninvasive pump flow estimation of a centrifugal blood pump," *Artif. Organs*, vol. 21, pp. 651–654, 1997.

[15] T. Tsukiya, Y. Taenaka, T. Nishinaka, M. Oshikawa, H. Ohnishi, E. Tatsumi, H. Takano, Y. Konishi, K. Ito, and M. Shimada, "Application of indirect flow rate measurement using motor driving signals to a centrifugal blood pump with an integrated motor," *Artif. Organs*, vol. 25, pp. 692–696, 2001.

[16] Y. W. Wong, W. K. Chan, S. C. M. Yu, and L. P. Chua, "Effects of scaling on centrifugal blood pumps," *Artif. Organs*, vol. 26, pp. 998–1001, 2002.

[17] M. Lorenz and W. A. Smith, "Rotodynamic pump scaling," *ASAIO J.*, vol. 48, pp. 419–430, 2002.

[18] T. Kitamura, Y. Matsushima, T. Tokuyama, S. Kono, K. Nishimura, M. Komeda, M. Yanai, T. Kijima, and C. Nojiri, "Physical model-based indirect measurements of blood pressure and flow using a centrifugal pump," *Artif. Organs*, vol. 24, pp. 589–593, 2000.

[19] D. M. Karantonis, S. L. Cloherty, D. G. Mason, P. J. Ayre, and N H. Lovell, "Noninvasive pulsatile flow estimation for an implantable rotary blood pump," in *Proc. 29th Annu. Int. Conf. IEEE Eng. Med. Biol.*, Lyon, France, Aug. 23–26, pp. 1018–1021.

[20] R. H. Sabersky, A. J. Acosta, and E. G. Hauptmann, *Fluid Flow*, 2nd ed. New York: Macmillan, 1971, p. 423.

Einly Lim received the B. BiomedE. (Hons.) and M.E. degrees from the University of Malaya (UM), Kuala Lumpur, Malaysia, in 2006. She is currently working toward the Ph.D. degree at the Graduate School of Biomedical Engineering, University of New South Wales, Sydney, Australia.

Her current research interests include modeling and control of an implantable rotary blood pump.

Dean M. Karantonis (S'05) received the B.E. (Hons.) degree in computer engineering and the M. BiomedE. degree in biomedical engineering in 2005 from the University of New South Wales (UNSW), Sydney, Australia, where he is currently working toward the Ph.D. degree at the Graduate School of Biomedical Engineering.

His current research interests include simulation and control of an implantable rotary blood pump.

John A. Reizes received the B.E., M.E., and Ph.D. degrees from the University of New South Wales (UNSW), Sydney, Australia, in 1960, 1965, and 1975, respectively.

He is currently an Adjunct Professor at the School of Mechanical and Manufacturing Engineering, University of New South Wales (UNSW), Sydney, Australia, and the Faculty of Engineering, University of Technology Sydney (UTS), Sydney. He is the author or coauthor of more than 170 papers. He was a Chairman of the College of Mechanical Engineers.

Dr. Reizes was a Past Editor of the *Mechanical Transaction* of the Institution of Engineers Australia, and currently, the Chairman of the Australasian Fluids and Thermal Engineering Society. He was on the Engineering 2 Panel of the Australian Research Council (ARC), and on the ARC Collaborative Grants Committee. He was the recipient of the 2006 AGM Michell Medal by the College of Mechanical Engineers of the Institution of Engineers Australia, its highest honor, for his contribution to the profession, sustained leadership in the development of mechanical engineering, and for his contribution to the art and science of mechanical engineering.

Shaun L. Cloherty (M'00) received the B.E. (Hons.) degree in aerospace avionics from the Queensland University of Technology, Brisbane, Australia, in 1997, and the Ph.D. degree in biomedical engineering from the University of New South Wales, Sydney, Australia, in 2005.

During 2005–2007, he was a Research Associate at the Graduate School of Biomedical Engineering, Sydney, where he was engaged in research on cardiac electrophysiology and modeling, flow estimation and modeling for control of an implantable rotary blood pump, and modeling of electrical stimulation strategies for a retinal vision prosthesis. He is currently a Postdoctoral Fellow in the Research School of Biological Sciences, Australian National University, Canberra, Australia. His current research interests include mammalian visual cortex and functional assessment of electrical stimulation strategies for a retinal vision prosthesis.

Dr. Cloherty is a Founding Officer of the New South Wales Chapter of the IEEE Engineering in Medicine and Biology Society, Sydney, Australia.

David G. Mason was born Fremantle, Western Australia on December 7, 1962. He received the Graduate degree in electrical and electronic engineering from the University of Melbourne, Melbourne, Australia, in 1985, and the Ph.D. degree in expert systems for closed-loop drug infusion systems in intensive care from the Royal Melbourne Hospital, Melbourne, in 1990.

He was earlier with Telectronics, Ltd., Sydney, where he was engaged in research on rhythm discriminators for implantable defibrillators, and later, with the University of London, London, U.K., where he developed endocardial electrodes for treatment of atrial flutter. During 2001, he was in Melbourne to develop an expert advisory system for circulatory management in intensive care. During 2004, he was engaged in research on feedback controller for a left ventricular assist device with Ventracor Limited. He is currently in the Department of Surgery, Monash University, Victoria, Australia, as a Senior Research Fellow.

Nigel H. Lovell (M'90–SM'98) received the B.E. (Hons.) and Ph.D. degrees from the University of New South Wales (UNSW), Sydney, Australia.

He is currently a Professor of Biomedical Engineering at the Graduate School of Biomedical Engineering, UNSW, and an Adjunct Professor in the School of Electrical Engineering and Telecommunications, UNSW. He is the author or coauthor of more than 250 refereed journals, conference proceedings, book chapters, and patents. His current research interests include cardiac modeling, home telecare technologies, biological signal processing, and visual prosthesis design.

Dr. Lovell was the IEEE Engineering in Medicine and Biology Society (EMBS) Vice-President (VP) for Conferences (2004/2005) and VP for Member and Student Activities (2002/2003). He was the Program Co-Chair for the Annual IEEE Engineering in Medicine and Biology Society (EMBS) Conference 2007 that was held in Lyon, France.